

# The structure and large-scale organization of extreme cold waves over the conterminous United States

Zuowei Xie<sup>1,2</sup>  · Robert X. Black<sup>1</sup> · Yi Deng<sup>1</sup>

Received: 26 August 2016 / Accepted: 30 January 2017 / Published online: 13 March 2017  
© Springer-Verlag Berlin Heidelberg (outside the USA) 2017

**Abstract** Extreme cold waves (ECWs) occurring over the conterminous United States (US) are studied through a systematic identification and documentation of their local synoptic structures, associated large-scale meteorological patterns (LMPs), and forcing mechanisms external to the US. Focusing on the boreal cool season (November–March) for 1950–2005, a hierarchical cluster analysis identifies three ECW patterns, respectively characterized by cold surface air temperature anomalies over the upper midwest (UM), northwestern (NW), and southeastern (SE) US. Locally, ECWs are synoptically organized by anomalous high pressure and northerly flow. At larger scales, the UM LMP features a zonal dipole in the mid-tropospheric height field over North America, while the NW and SE LMPs each include a zonal wave train extending from the North Pacific across North America into the North Atlantic. The Community Climate System Model version 4 (CCSM4) in general simulates the three ECW patterns quite well and successfully reproduces the observed enhancements in the frequency of their associated LMPs. La Niña and the cool phase of the Pacific Decadal Oscillation (PDO) favor the occurrence of NW ECWs, while the warm PDO phase, low Arctic sea ice extent and high Eurasian snow cover extent (SCE) are associated with elevated SE-ECW frequency. Additionally, high Eurasian SCE is linked to increases in the occurrence likelihood of UM ECWs.

**Keywords** Extreme cold wave · Large-scale meteorological pattern · Pacific decadal oscillation · Sea ice · Snow cover

## 1 Introduction

During boreal winter extreme cold waves (ECWs) can pose a great threat to human lives, economies and societies (IPCC 2012). The frequency, intensity, spatial extent, duration, and timing of extreme weather events are thought to vary in association with climate change, resulting in unprecedented extreme weather events (IPCC 2012). It has been recognized that over continental regions there has been an increased frequency of unusually cold winter months since the end of the 1990s (Westby et al. 2013; Cohen et al. 2014). A large number of record-breaking extreme events have been reported in recent years (Bueh et al. 2011; WMO 2012; Wolter et al. 2015). For example, the frigid winter of 2013/14 provided the central and eastern United States (US) with the most intense ECW in decades (Wolter et al. 2015; Trenary et al. 2015; Hartmann 2015). In February 2015, the Midwest and Northeast US suffered both ECWs and record setting snowstorms (Bosart et al. 2015). The antecedent circulation patterns favoring ECWs range from synoptic weather disturbances to planetary-scale climate modes and remote forcing (Westby et al. 2013; Cohen et al. 2014; Hartmann 2015; Bosart et al. 2015; Grotjahn et al. 2015).

ECWs are organized by large-scale meteorological patterns (LMPs), which have a spatial scale generally larger than synoptic but smaller than planetary-scale climate modes (Grotjahn et al. 2015). Generally speaking, ECWs are associated with overlying negative anomalies in 500 hPa geopotential height and anomalous upstream

✉ Zuowei Xie  
zuowei.xie@eas.gatech.edu

<sup>1</sup> School of Earth and Atmospheric Sciences, Georgia Institute of Technology, Atlanta, GA 30332, USA

<sup>2</sup> International Center for Climate and Environment Sciences, Institute of Atmospheric Physics, Chinese Academy of Sciences, Beijing 100029, China

surface high pressure (Loikith and Broccoli 2012; Westby and Black 2015). Carrera et al. (2004) found that Alaskan blocking events lead to ECWs over the southern US plains. In addition, Whan et al. (2016) found that a high blocking frequency over the North Pacific increases the occurrence frequency and spatial extent of ECWs over the southwestern US. Stan and Straus (2007) classified four large-scale circulation regimes over western Northern Hemisphere and noted that two regimes (i.e., Alaskan ridge and Arctic high) are associated with ECWs over North America. In contrast to such ECW studies beginning with LMPs, Konrad (1996) performed a synoptic climatology of ECWs and discovered a positive relationship between ECW intensity over the southeastern US and LMP persistence. Bosart et al. (2015) showed that a persistent amplified LMP, characterized by high-amplitude ridge and deep trough structures over western and eastern North America, respectively, supported the abnormally high recurrence of heavy snowstorms over the northeastern US during February 2015. Grotjahn et al. (2015) reviewed existing research on ECW LMPs for the US and note that our current scientific knowledge of the synoptic and dynamic nature of LMPs is generally lacking. This review paper emerged from a US CLIVAR workshop on the large-scale organization of US weather extremes (Grotjahn et al. 2014). To address this deficiency, the current study systematically investigates ECWs over the conterminous US along with their associated LMPs.

A number of studies have examined potential remote forcing of ECW occurrence. Loikith and Broccoli (2014) found a weak connection between El Niño Southern Oscillation (ENSO) and extreme temperature days over the US. The Pacific Decadal Oscillation (PDO) influences ECW occurrence over the northwestern US (Kenyon and Hegerl 2008; Westby et al. 2013). Emphasizing extratropical regions, Cohen et al. (2014) suggested that sea ice and snow cover jointly influence extreme weather over mid-latitude. Liu et al. (2012) concluded that the decline of Arctic sea ice can enhance ECW frequency. Francis and Vavrus (2012) and Kug et al. (2015) suggested that sea-ice loss may act to slow the eastward progression of Rossby waves in the upper troposphere, resulting in prolonged extreme weather events. Westby et al. (2013) found that the regional impact of the PDO and ENSO on US ECWs mirror one another, reflecting a commonality in their LMP structure over North America. Cohen et al. (2014) summarized three pathways linking Arctic climate change with ECWs. Given the above noted associations between remote forcing and ECWs, there is a strong existing need for more comprehensive examination of such linkages with a focus on the intermediate role played by LMPs.

The Coupled Model Intercomparison Projects's fifth phase (CMIP5) has been adopted to evaluate the model skill of ECWs (Grotjahn et al. 2015). Westby et al. (2013)

examined ECW behavior and planetary climate mode-ECW linkages in CMIP5 models. They found that both ECW frequency and modulation of ECW frequency by planetary climate mode are generally underestimated in CMIP5 models. Adopting an Expert Team on Climate Change Detection and Indices approach, Sillmann et al. (2013) assessed the CMIP5 representation of climate extremes and found that the CMIP5 models are generally able to simulate climate extremes and their trend patterns. Although aspects of ECW behavior in CMIP5 models have been examined in these studies, the corresponding skill of CMIP5 models in represented ECW LMPs is lacking.

We note that most prior studies of ECWs are based on either individual regional events (e.g., the recent events discussed earlier) or events occurring at individual grid points and/or within pre-selected regions (e.g., the review of Grotjahn et al. 2015), leading to implicit a priori assumptions regarding spatial structure and affected regions. In the current study we first expand on the prior studies of ECW events by applying a cluster analysis to systematically identify the primary ECW patterns occurring over the conterminous US during the boreal cool season. We then use this classification to additionally isolate their associated LMPs and potential linkages to anomalous remote forcing. The associated LMPs are characterized using composite 500 hPa geopotential height (Z500) anomaly patterns that, in turn, are used to define daily LMP indices (related to the spatial correlation with the daily Z500 anomaly field). Parallel analyses of ECW circulation features and LMP indices in historical CCSM4 simulations are also examined. Linkages among ECWs, LMPs and remote forcing are studied in the context of the occurrence and projection index of ECWs. In the following section, we describe the data and methodology. In Sect. 3, we present the circulation patterns and metrics for the different ECW types and their representation in CCSM4. In Sect. 4, the relationships among ECWs and ENSO, PDO, sea ice extent (SIE) and snow cover extent (SCE) are discussed. A summary and discussion are provided in the final section.

## 2 Data and methodology

### 2.1 Data

The daily mean observational data used in the present study comes from the National Centers for Environmental Prediction-National Center for Atmospheric Research Reanalysis (Kalnay et al. 1996) for the boreal cool season (November 1st to March 31) from 1950 to 2005. The variables studied here include 2-m surface air temperature (SAT), sea level pressure (SLP), 500 hPa geopotential height (Z500), and horizontal winds at 10 m (surface) and 500 hPa. Surface

data are provided in a T62 Gaussian grid with  $194 \times 94$  points, while the 500 hPa data has a resolution of  $2.5^\circ$  latitude by  $2.5^\circ$  longitude.

The remote forcing measures of interest are ENSO, PDO, Arctic SIE and Eurasian SCE, all recognized as potentially influencing ECW occurrence. ENSO events are defined using observed sea surface temperature (SST) from the National Oceanic and Atmospheric Administration (NOAA) Enhanced Reconstructed Sea Surface Temperature version 4 (Huang et al. 2015). Following the Climate Prediction Center method, we define the Oceanic Niño Index as the cool-season mean of SST anomalies within the Niño 3.4 region of  $5^\circ\text{N}$ – $5^\circ\text{S}$ ,  $120^\circ$ – $170^\circ\text{W}$  (e.g., see [http://www.cpc.ncep.noaa.gov/products/analysis\\_monitoring/ensostuff/ensoyears.shtml](http://www.cpc.ncep.noaa.gov/products/analysis_monitoring/ensostuff/ensoyears.shtml) for more details). We use the NOAA PDO index, which is computed by projecting SST anomalies onto the corresponding PDO map (<https://www.ncdc.noaa.gov/teleconnections/pdo>). A measure of SIE for the Arctic is obtained from the National snow and Ice Data center for the period from 1978 to 2005, which is derived from the passive satellite microwave-derived data (Fetterer et al. 2002). Since there is a declining trend in SIE (Cohen et al. 2014), we calculate the monthly SIE index for the cool season and then remove the long-term linear trend. We also assess the monthly mean SCE over Eurasia using a satellite-derived measure (Robinson et al. 1993) for the period 1966–2005. Since there is an increasing (decreasing) trend in Eurasian SCE after (before) 1980 (Cohen et al. 2014), we calculate the monthly SCE index for the cool season and then remove the least squares quadratic fit. The cool-season index for each remote forcing measure is then correspondingly normalized.

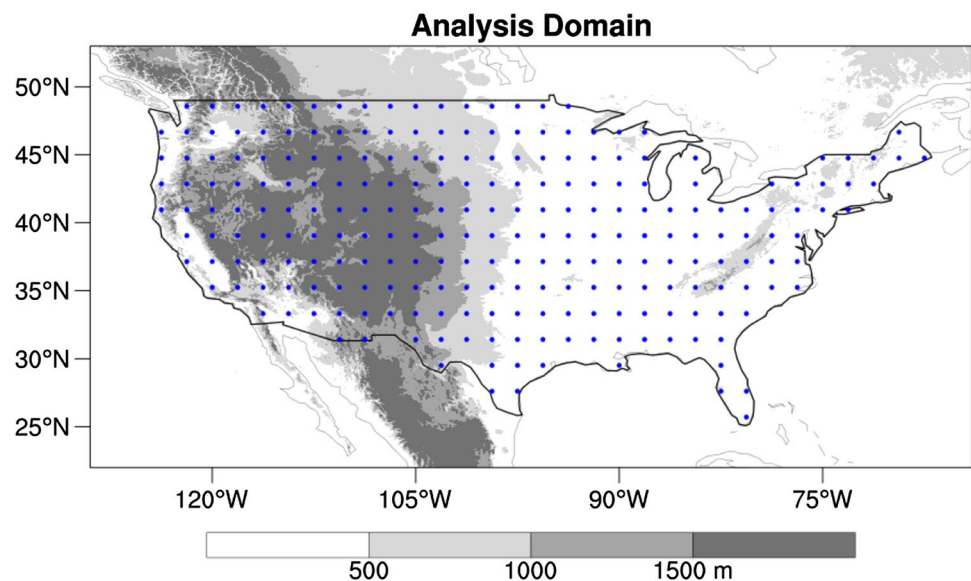
To test the capability of Community Climate System Model version 4 in representing ECW characteristics,

including ECW occurrence and LMP behavior, we analyze the same fields as in observations but from a historical simulation provided on a  $1.25^\circ \times 0.9^\circ$  longitude-latitude grid (Gent et al. 2011). Output from the CCSM4's historical climate experiments (ensemble r6i1p1) is compared with observations for the same period (1950–2005). To facilitate a direct comparison with observations, CCSM4 output data are first re-gridded to the coarser observation grid using a local area averaging. Adopting a uniform grid size for both the modeled and observed datasets enables a more direct quantitative comparison of the parallel results.

## 2.2 Definition of extreme cold waves events

ECW are identified in terms of local daily SAT anomalies (relative to the long-term daily climatology of 1950–2005) at 237 grid points in the conterminous US (Fig. 1), similar to Westby et al. (2013). Individual ECW events are isolated using the following four criteria: (1) an extreme cold SAT *grid point* is recorded when the normalized SAT anomaly falls below  $-1.5 \sigma$  (sigma, the standard deviation in the daily-mean SAT for the calendar day); (2) an extreme cold SAT day is additionally recorded if the total number of extreme cold SAT grid points exceeds 10% of the total number of grid points (237); (3) an ECW *event* is recorded when there are 3 or more successive extreme cold SAT days; (4) the interval between peak days (the day within each ECW event when the total number of extreme cold SAT grid points is largest) of two events is required to be at least 8 days. This procedure isolates ECW events having a long-lasting and widespread impact. Following this approach, we identify 276 observed ECW events (covering 1626 days) and 261 CCSM4 events (covering 1792 days).

**Fig. 1** The analysis domain of the conterminous US and the distribution of 237 grid points (dotted) used in the analysis. Shaded areas indicate topography (see scale at bottom, m)



### 2.3 Classification of extreme cold waves

After identifying the ECW events, they are then categorized by applying Agglomerative Hierarchical Clustering (Wilks 2006; Park et al. 2013) to the corresponding fields of normalized SAT anomalies over the conterminous US (i.e., all 237 grid points). Initially, an object is defined as the pattern of 237 grid points of SAT anomalies occurring on each cold SAT day within each ECW event and each single object is considered as a cluster. Then, we compute Ward’s distance between each pair of clusters (Ward 1963), and merge two clusters together where the Ward’s distance is smallest. Therefore, the total number of clusters decreases by one in this merger. Finally, the same procedure is sequentially repeated for each new group of clusters until all clusters merges into one cluster (Fig. 2a). Considering the curve line of the smallest Ward’s distance (Fig. 2b), there is a substantial “jump”, which indicates that the patterns of two clusters merged at this step are considerably different from one another and thereby they should not be merged. Following this procedure, we identify three distinct ECW groups in both observations and the CCSM4 simulations. Readers are referred to Park et al. (2013) and Zhao et al. (2016) for more details.

To test the robustness of the ECW clusters identified from observations, we have performed three sensitivity experiments by perturbing (1) the threshold criterion for an extreme cold SAT *grid point* (−1 standard deviation versus −2 standard deviations), (2) the minimum areal

coverage (over the US) required for an extreme cold SAT day (15% versus 20%), and (3) the cool season duration (October–February versus December–April). The results (not shown) indicate that the ECW patterns identified are qualitatively insensitive to the specific parameter choice. The main differences obtained were in the anomaly pattern magnitude (to be expected in sensitivity test #1) and the relative frequency of occurrence (to be expected in sensitivity test #3).

### 2.4 Rossby wave-activity flux

The horizontal energy propagation of quasi-stationary Rossby waves is assessed using the wave-activity flux defined by Takaya and Nakamura (2001) and expressed as

$$W = \frac{p}{2000|U|} \begin{bmatrix} u(v'^2 - \psi'v'_x) + v(-u'v' + \psi'u'_x) \\ u(-u'v' + \psi'u'_x) + v(u'^2 + \psi'v'_y) \end{bmatrix}, \quad (1)$$

where  $\psi'$  denotes perturbation geostrophic stream function,  $u' = (u', v')$  perturbation geostrophic wind velocity,  $U = (U, V)$  a basic state horizontal flow velocity, and  $p$  is pressure normalized by 1000 (hPa). Climatological mean values of Z500 and horizontal 500 hPa winds are calculated in a similar manner to SAT (see earlier discussion). The basic state flow in the wave-activity flux analysis is taken to be the cool-season average of climatological mean. For each ECW, daily perturbation values are obtained by removing the corresponding daily climatological mean value.

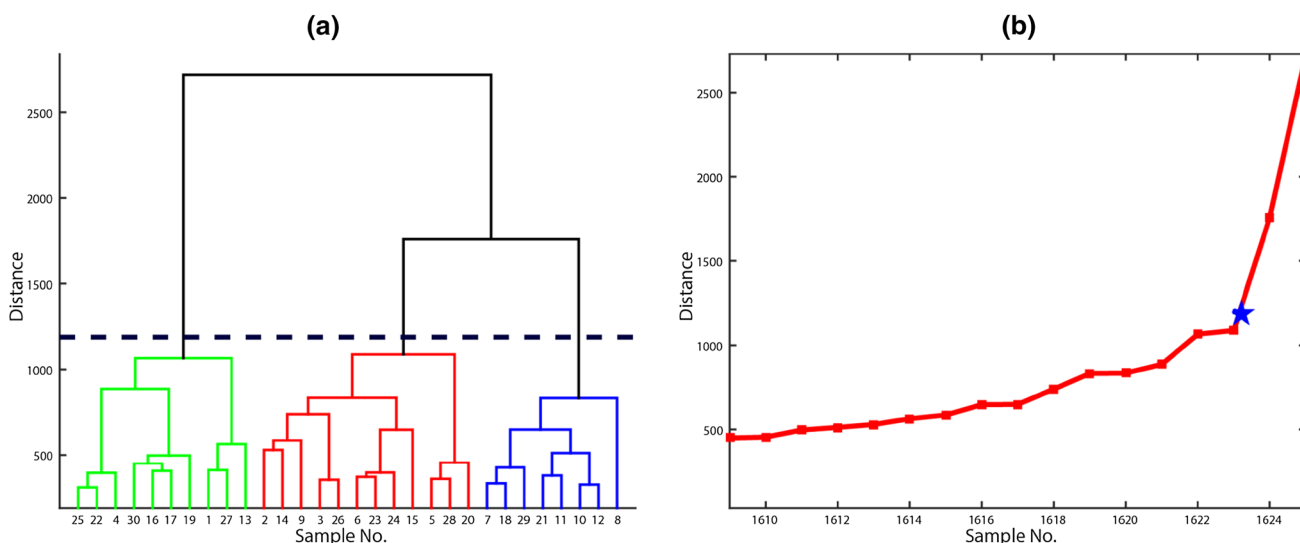


**Fig. 2** a Dendrogram representation for the complete-linkage hierarchical clustering of ECWs and b Ward’s distance between each pair of clusters. The dashed line in a and blue star in b indicates the procedural cutoff at three clusters

### 3 ECW features and their representation in CCSM4

#### 3.1 Classification

Figure 3 shows the composite SAT anomaly patterns for ECWs obtained from observations and CCSM4, respectively. It should be noted that the SAT anomaly and the SLP and Z500 anomaly fields that follow are composited in terms of ECW days. The statistical significance of composite anomalies is assessed by applying a Student's *t* test (Wilks 2006). Since surface wind data is unavailable from the CCSM4 output, surface wind anomalies are displayed only for observations. Three distinct ECW patterns are identified for the region of interest (the conterminous US). It is useful to first

note that, even though the events are identified in terms of their net impact upon the US, the patterns identified are clearly not restricted to this domain. For observed events, the most common ECW pattern is characterized by predominantly negative SAT anomalies covering most of the US and southern Canada with a large amplitude center over the upper midwest US (Fig. 3a). This pattern is associated with widespread northerly surface wind anomalies extending from the Arctic through North America to the Gulf of Mexico, serving to transport cold air into North America. The second ECW pattern features a cold SAT anomaly over the northwestern and western coast of US with the strongest impact over the northern Rocky Mountains (Fig. 3b). This SAT feature is linked to anomalous northeasterly flow that helps to transport cold air from the Canadian interior toward the

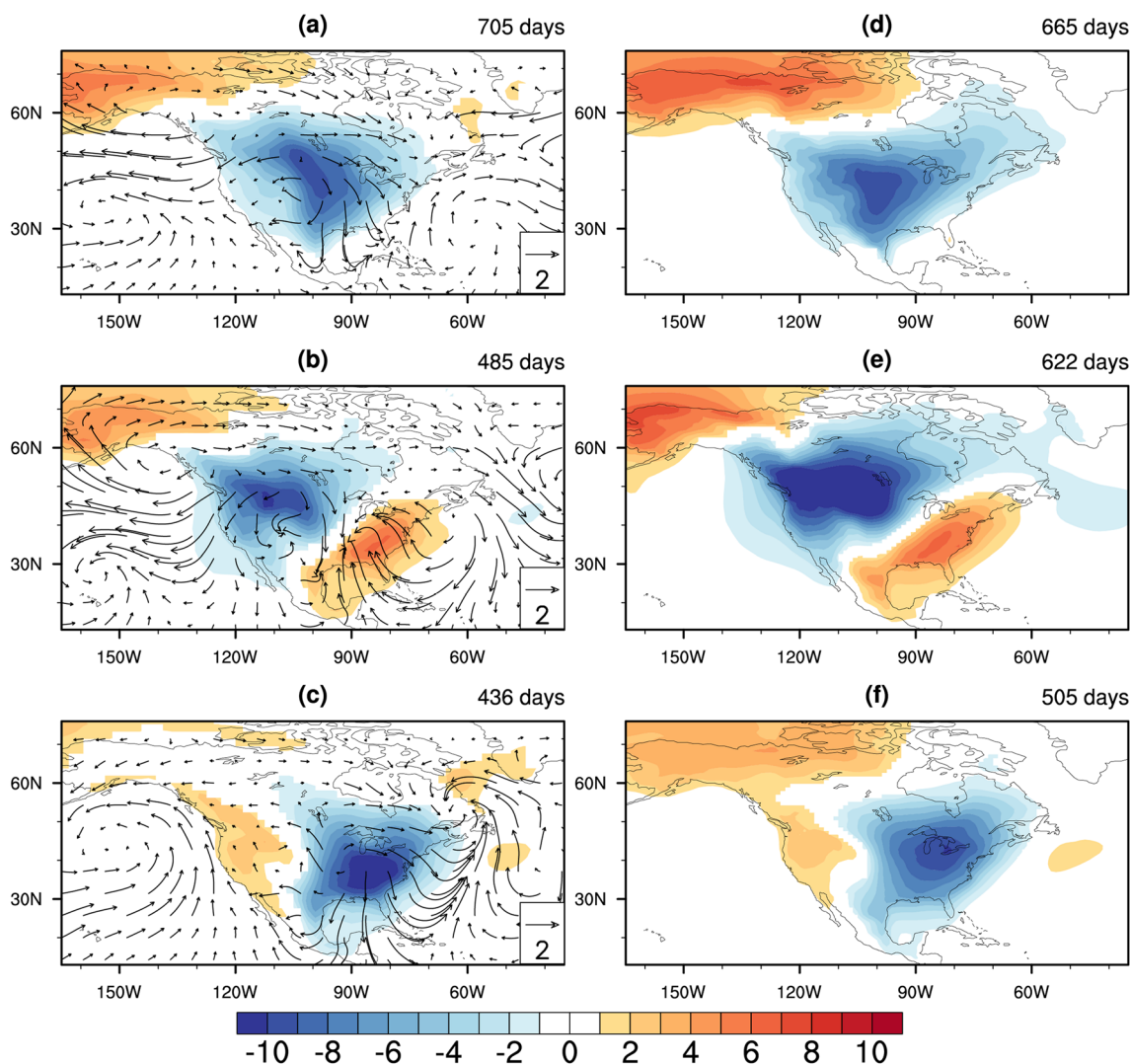


**Fig. 3** Composite SAT anomalies (*Shaded*; °C) and surface horizontal wind anomalies (*arrows*, see scale at *bottom*) of **a** UM-, **b** NW-, and **c** SE-ECW groups for observations. Only composite anomalies

that are statistically significant at 95% confidence are shaded. **d–f** as per **a–c**, but for CCSM4

northwest US coast. In addition, a prominent warm anomaly feature is found to extend from Texas to the Mid-Atlantic, in response to anomalous southerly and southeasterly flow extending from the Gulf of Mexico and the North Atlantic. The third ECW pattern strongly impacts the entire eastern US and southeastern Canada with a pronounced impact on the southeastern US (Fig. 3c). The northerly wind anomalies are mainly concentrated over eastern North America, suggesting a more local, in situ development. Given the respective distributions of cold SAT anomalies, these three ECW clusters are subsequently denoted the upper midwest (UM)-, northwest- (NW)-, and southeastern (SE)-ECW patterns.

Although the corresponding CCSM4 ECW patterns strongly resemble those of observations, they differ in geographic extension and magnitude (Fig. 3d–f). For the leading two patterns, the CCSM4 cold SAT anomaly pattern extends further northeast into the Labrador Sea compared to observations (Fig. 3d, e). For the NW-ECW cluster, the CCSM4 central anomaly amplitude is notably stronger than for observations. In contrast, the central anomaly magnitude for the SE ECWs is anomalously weak in CCSM4. In addition, for this pattern the cold SAT core is centered near the Great Lakes, which is shifted northward compared to the observed structure.

Table 1 shows the total number of days each ECW pattern occurs in both observation and CCSM4. It is first evident that the total frequency of ECW days in CCSM4 is about 10% greater than observed. Moreover, the respective ECW frequency is more evenly distributed among the three CCSM4 clusters than in observations. More specifically, in observations the frequency of UM ECW (705 days) accounts for 43.4% of the total, considerably more than that in CCSM4. In contrast, both the relative and absolute frequency of NW and SE ECWs are notably greater in CCSM4 than in observations, particularly for SE-ECW days. The analysis indicates that the CCSM4 may overpopulate the NW and SE ECWs (even though their spatial structure is fairly well replicated by the model).

### 3.2 Circulation features

Figure 4 shows composite SLP anomalies for the three ECW clusters. In both observations and the CCSM4, the SLP anomaly patterns for all three clusters exhibit anomalous high pressure patterns over North America, located near and to the west of cold SAT anomaly center. Focusing first

on observations, the UM-ECW cluster (Fig. 4a) is linked to a broad high SLP anomaly pattern that extends from Alaska to the south central US along with significant anomalies extending into the Arctic. The core of this pattern extends southward along the lee side of the Rocky Mountains, which favors the establishment of robust cold anomalies over the upper midwest US (Westby and Black 2015). The positive SLP anomaly pattern for the NW-ECW cluster bears some similarity to that of the UM-ECW group, but is more zonally oriented (extending from the Gulf of Alaska to western Canada) and shifted northwestward (Fig. 4b). In contrast, for the SE-ECW cluster (Fig. 4c), the high pressure anomaly pattern is more localized over the central and eastern US with a meridionally elongated structure.

The corresponding pressure anomaly patterns in CCSM4 are basically consistent with those found in observations (Fig. 4d–f). However, they differ somewhat from the observed patterns in terms of amplitude and regional structural details. For the UM ECWs (Fig. 4d), the high pressure anomaly pattern is not only stronger in amplitude, but also extends more broadly over the US. As a result, the CCSM4 pressure pattern is likely to induce a more intense and broader cold SAT anomaly pattern over the US, consistent with our earlier discussion of Fig. 3. Likewise, for the NW ECWs (Fig. 3e), the CCSM4 pressure pattern is considerably stronger in terms of amplitude and has a broader meridional extent, leading to a stronger cold SAT anomaly pattern with greater areal coverage US. In contrast, for the SE ECWs, although significant high-pressure anomalies extend more broadly over North America, they are notably weaker than observations, consistent with weaker SAT anomalies in CCSM4.

Figure 5 displays the composite Z500 anomalies and corresponding 500 hPa Rossby wave activity flux for the three ECW groups. The analysis results indicate that the anomalous large-scale meteorological pattern (LMP) encompassing each ECW type exhibits a distinct Rossby wave structure. Focusing first on observed ECWs, the UM LMP features a significant positive height anomaly centered over Alaska along with a downstream negative height anomaly located over central and southeastern North America. Both features are longitudinally broad and there is evidence of modest Rossby wave energy propagation from the ridge southeastward toward the downstream low (Fig. 5a), noting that the wave activity flux denotes energy propagation and not phase propagation. In contrast, the LMP of NW-ECW category features a quasi-zonal wave train of height anomalies extending from near Alaska eastward through North America into the North Atlantic, marked by a conspicuous positive height anomaly center over the Gulf of Alaska and a deep negative height anomaly center over the Rocky Mountains (Fig. 5b). The individual anomaly features embedded within this wavetrain are closer to synoptic-scale

**Table 1** The number of days for each ECW clusters

	Cluster 1	Cluster 2	Cluster 3	Total
Observation	705	485	436	1626
CCSM4	665	622	505	1792

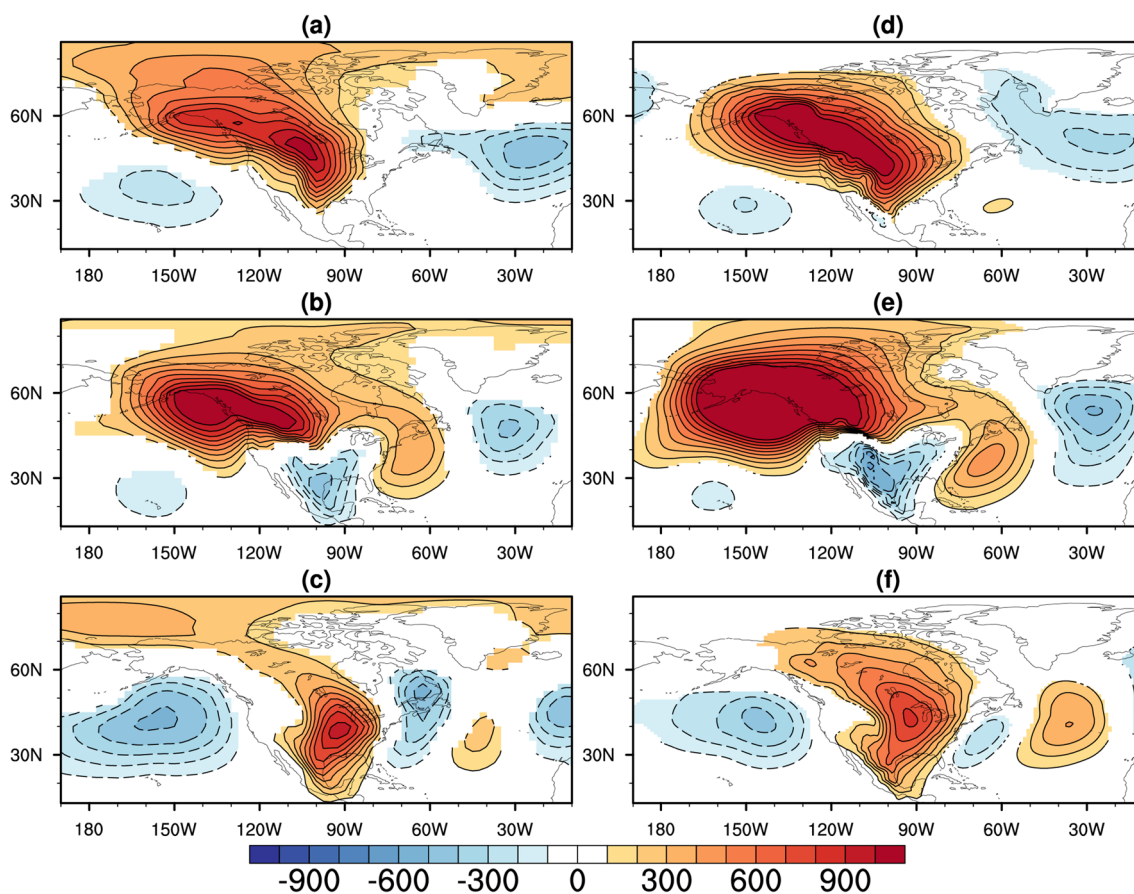


**Fig. 4** Composite sea level pressure anomalies of **a** UM-, **b** NW-, and **c** SE-ECW groups for observations. Only composite anomalies that are statistically significant at 95% confidence are shaded and contoured. **d–f** as per **a–c**, but for CCSM4

eddies in both size (spatial scale) and structure (evidence of meridional elongation). It is noteworthy that this wave-train LMP is linked to robust eastward Rossby wave energy propagation, strongly suggesting that the downstream components of the LMP are remotely forced. The NW LMP coincides with the Alaskan blocking circulation (Carrera et al. 2004), known to induce ECWs in the northwest US. The SE-ECW group (Fig. 5c) is characterized by a height anomaly pattern that is qualitatively out of phase with respect to the LMP of NW-ECW cluster. However, the pattern is more zonally oriented in structure and appears more regionally localized in terms of magnitude (the most prominent feature being the anomalous low over the eastern US). This localization is also evident in the wave activity flux pattern that indicates a primary wave source over North America with only weak remote forcing from upstream. To some extent, the SE LMP is in phase with an Arctic high regime related to ECWs over the southeastern US (Stan and Straus 2007). Stan and Straus (2007) point out that these regimes are not necessarily associated with ECWs. Since our study begins with ECWs, it effectively isolates LMPs that are more typically linked to ECWs including

Alaskan blocking/ridge, Arctic high pressure, etc. As discussed by Westby et al. (2013), ECW occurrence over the northwestern (southeastern) US tends to be abnormally frequent during the negative (positive) phase of the PNA pattern. It might be anticipated that, on longer time scales, the LMP of the NW- and SE-ECW groups may be affected by Pacific SST forcing via the PNA-like pattern, which will be discussed further in the following sections.

The LMPs isolated here bear some resemblance to those identified by Grotjahn and Faure (2008) and Loikith and Broccoli (2014). In their studies, the LMPs are extracted based on ECW occurrence at a city or individual grid points. In contrast, in the present study, ECWs are more broadly defined in terms of net event impact in the region of interest without a priori assumptions regarding spatial structure and affected regions. Such an approach will capture the most common widespread ECWs and tends to reflect the impact of organized large-scale circulation patterns. It should be noted that none of the cold core centers discovered in our three ECW groups coincide with the pre-selected locations of Grotjahn and Faure (2008) or Loikith and Broccoli (2014). In fact, the LMPs identified in the

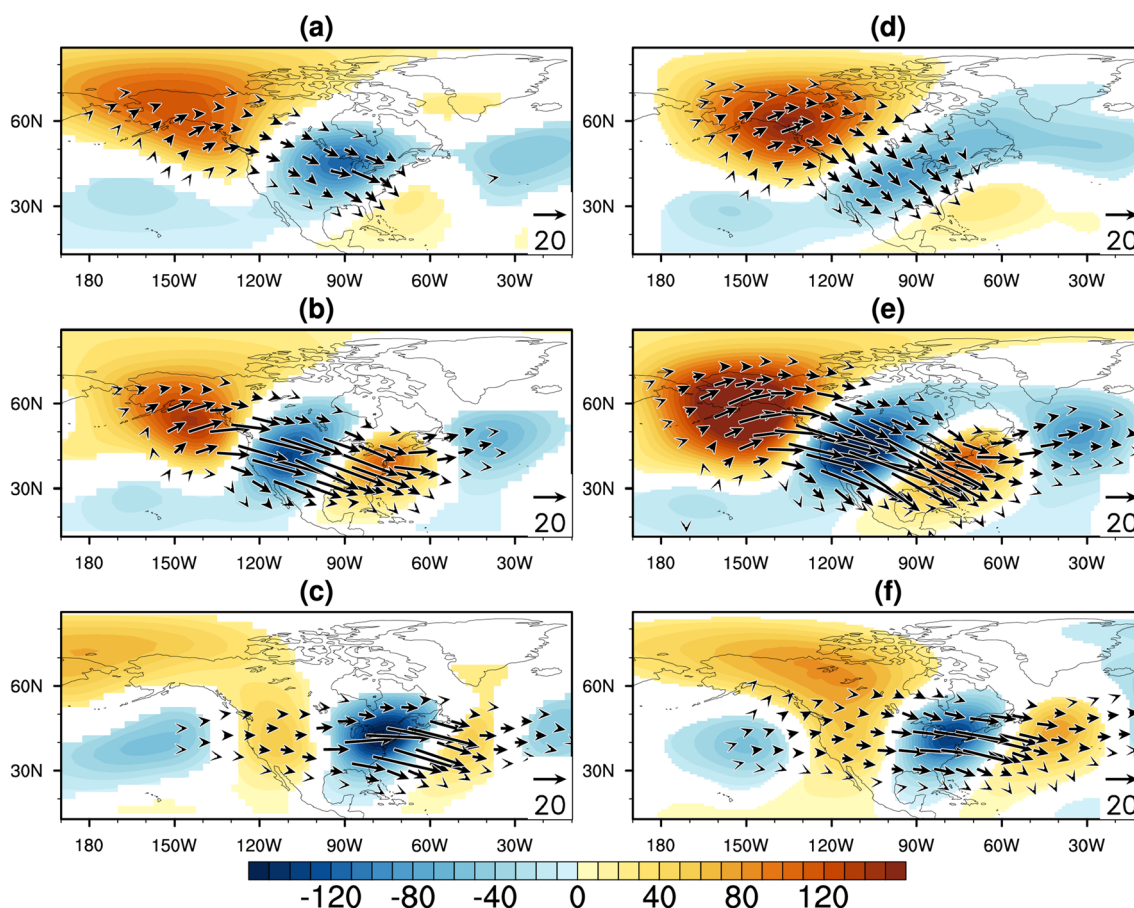


**Fig. 5** Composite Geopotential height anomalies (*shading*, see *scale bar* at *bottom*) and wave activity fluxes (*arrows*, units of  $\text{m}^2 \text{s}^{-2}$ ; see *scale* at the *bottom*) at 500 hPa of **a** UM-, **b** NW-, and **c** SE-ECW groups for observation. Only composite anomalies that are statisti-

cally significant at 95% confidence are shaded. *Arrow* magnitudes less than  $3 \text{ m}^2 \text{ s}^{-2}$  are omitted for clarity. **d–f** as per **a–c**, but for CCSM4

current study differ rather substantially from their counterparts in the earlier studies, both in terms of regional structure and location. For example, the negative height anomaly feature over the Rocky Mountains identified for the NW-ECW group extends spatially more broadly than that identified in Grotjahn and Faure (2008). Also, the prominent negative height anomaly features found for UM and SE ECWs are displaced westward compared to those found for ECWs over the Great Lakes and Gulf Coast as defined in Loikith and Broccoli (2014).

Compared to observed structures, although LMPs in CCSM4 correspond qualitatively well with observed events, the CCSM4 tends to reproduce LMPs with a stronger amplitude (Fig. 5d–f). Also, the lateral Rossby wave energy propagation in CCSM is more prominent than found in observations. In association with the enhanced Rossby wave signatures, the CCSM4 produces relatively conspicuous height anomalies over the North Atlantic downstream of the primary LMP. In particular, the CCSM4 NW LMP is considerably stronger in amplitude than in

observations (Fig. 5b, e). For the UM LMP in CCSM4 (Fig. 5d), the positive height anomaly over the Alaskan peninsula is higher in amplitude, while the downstream negative height anomaly feature is weaker in amplitude and exhibits an elongated anomaly structure extending from the North Pacific to the North Atlantic. In the CCSM4 SE LMP, the positive height anomaly center over northwestern Canada is displaced northward with respect to the observed structure. At the same time, the amplitude of the downstream negative height anomaly over eastern North America is weaker than observed.

### 3.3 Representation of the LMP index in CCSM4

Although we have shown general circulation anomaly features for the ECW groups in terms of composite meteorology fields, we still do not know the extent to which the CCSM4 represents the typical daily behavior of observed LMPs. In order to examine the representation of LMPs in CCSM4, we use each composite Z500 anomaly



pattern derived from observed ECW events (i.e., the Z500 patterns displayed in the left-hand column of Fig. 5) as a fundamental basis pattern to calculate a scalar metric of LMP occurrence. More specifically, a daily LMP index is constructed by projecting each daily Z500 anomaly pattern ( $Z'$ ) upon the basis pattern for each LMP ( $Z'_{LMP}$ ) over the domain encompassing  $10^{\circ}$ – $85^{\circ}$ N  $170^{\circ}$ E– $10^{\circ}$ W according to

$$\text{LMP index} = \frac{\text{cov}(Z'_{LMP}, Z')}{\sigma_{Z'_{LMP}} \times \sigma_{Z'}} \times \frac{\sigma_{Z'}}{\sigma_{Z'_{LMP}}} = \frac{\text{cov}(Z'_{LMP}, Z')}{\text{var}_{Z'_{LMP}}}. \tag{2}$$

This LMP index, which represents a modified pattern correlation, simultaneously measures both LMP phase and amplitude for each day. Linear regression maps of SAT anomaly patterns based upon the three daily LMP indices (not shown) are consistent with the composite result shown in Fig. 3. Probability density functions (PDF) for the three LMP indices are displayed in Fig. 6 for both observations and CCSM4. The first row presents the PDF distributions for all cool season days considered, while the second row presents PDF distributions restricted to *only those days* in which a specific ECW cluster is populated. A two-sample Kolmogorov–Smirnov test is adopted to examine whether there is a significant

difference between the probability distributions of two samples at 95% confidence (Wilks 2006).

First considering LMP distributions for the entire cool season, we note that for the UM and NW LMPs (Fig. 6a, b), the CCSM4 PDF distributions exhibit lower kurtosis and more highly populated distribution tails than found in observations. This suggests that the CCSM4 is inclined to produce higher-amplitude UM and NW LMPs. In contrast, the CCSM4 PDF for the SE LMP almost perfectly aligns with observations (Fig. 6c).

The ECW cluster-specific distributions (Fig. 6d–f) are generally negatively skewed and positively shifted, with peak frequency (mode) values near 1.0 for observations (reinforcing the notion that ECW occurrence is preferentially favored during the positive phase of the respective LMP). Compared to the observed distributions, the CCSM4 PDFs exhibit differences in both kurtosis and shift. Specifically, the UM LMP index exhibits lower kurtosis, likely reflecting the fact that the CCSM4 LMP is weaker in amplitude over the central US than found in observations. Noting that the CCSM4 has fewer UM-ECW days, this suggests a partial compensation between the CCSM4’s tendency to (a) overpopulate the UM LMP (Fig. 6a) and (b) underrepresent the UM LMP amplitude (Fig. 5d). In contrast, the PDF of NW LMP index is markedly right-shifted (more positive,

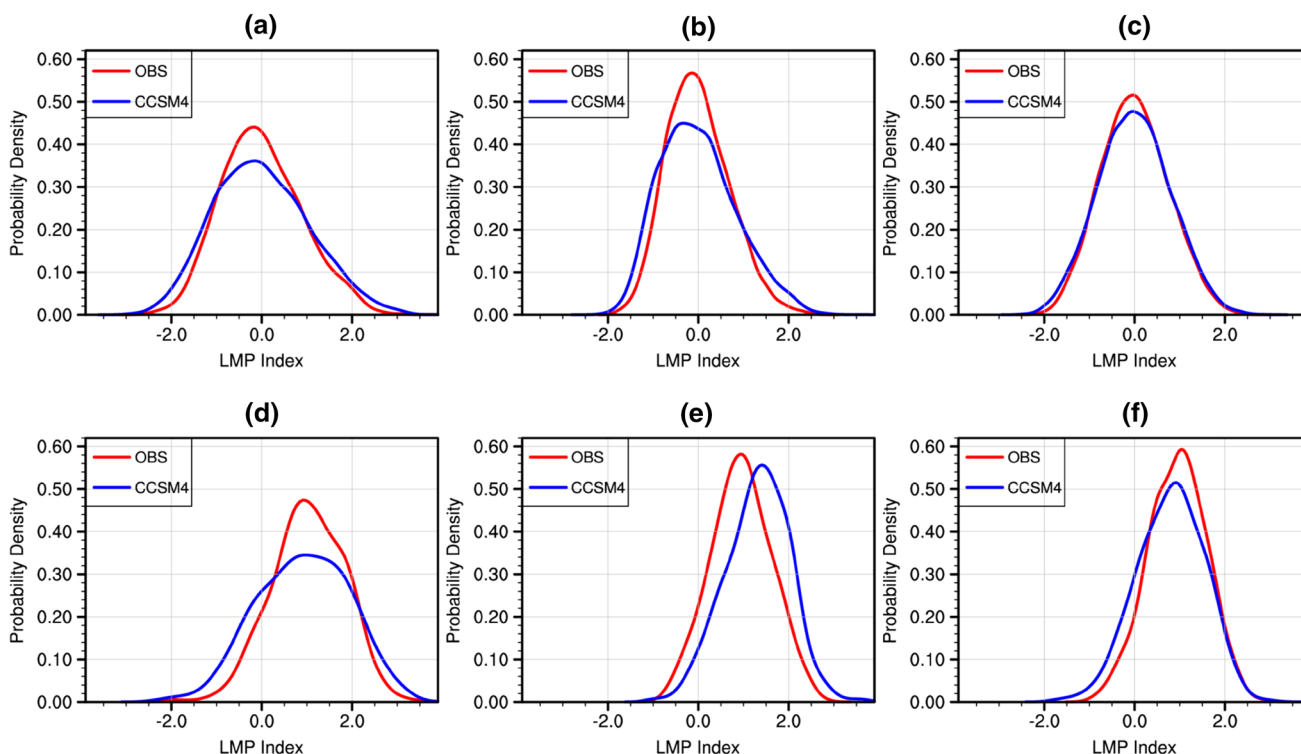


**Fig. 6** PDF of LMP indexes for **a** UM-, **b** NW- and **c** SE-ECW groups in observations (*red*) and CCSM4 (*blue*). **d–f** as per **a–c**, but for only those days within specific ECW cluster

Fig. 6e), consisting with the aforementioned observation that the CCSM4 LMP amplitude for NW ECW is anomalously strong (Fig. 5b, e). Since the frequency of NW-ECW days in CCSM4 is greater than observations, it might be concluded that this is simply related to an overpopulation of the NW LMP by CCSM4. Finally, for SE LMP, the CCSM4 kurtosis is lower than for observations, leading to larger LMP index spread or variability. One interpretation of this result is a weaker role for the SE LMP in model events, noting the higher frequency of SE-ECW days in CCSM4.

### 4 Association with remote forcing

In this section, we study the statistical relationship among remote forcing measures (such as ENSO, PDO, SIE and SCE) and ECWs. To extract prominent influences of remote forcing upon the atmospheric circulation, we have selected years in which the seasonal mean remote forcing indices are either above +1 or below -1 standard deviation, as shown in Table 2.

**Table 2** The years for the positive- and negative phases of remote forcing

	Positive phase	Negative phase
ENSO	1957, 1965, 1972, 1982, 1986, 1991, 1997	1955, 1970, 1973, 1975, 1988, 1995, 1998, 1999
PDO	1957, 1969, 1976, 1980, 1983, 1985, 1986, 1997, 2002	1950, 1951, 1955, 1956, 1961, 1970, 1971, 1973, 1975, 1990, 1999
SIE	1978, 1986, 1992, 1993, 1997	1979, 1980, 1983, 1995, 2003, 2004
SCE	1970, 1977, 1984, 1985, 2002	1967, 1974, 1975, 1979, 1980, 1988, 1989, 2001

### 4.1 Association with ENSO

Figure 7 displays the occurrence of ECWs along with sample PDFs for the NW LMP index, both stratified according to ENSO phase for the boreal cool season. The difference in magnitude between each pair of frequency bars is tested using a two-sample *t* test (Wilks 2006). In this case, occurrence frequency is normalized by the number of years for each ENSO phase. We find that NW ECWs are marginally more frequent during La Niña events than either El Niño or neutral years (Fig. 7a). We note, however, that the PDF of NW LMP index (Fig. 7b) is not significantly different during La Niña years versus neutral years. Instead, the PDF is left-shifted (more negative) during El Niño. The results suggest that ENSO likely modulates NW-ECW frequency via the NW LMP. Our findings expand upon the results of Loikith and Broccoli (2014), who found a slight increase in extreme cold minimum temperature months over the Rocky Mountains in association with La Niña.

### 4.2 Association with PDO

Figure 8 shows the occurrence of ECWs and PDFs for NW and SE LMP indexes stratified according to PDO phase for the boreal cool season. As seen from Fig. 8a, NW ECWs

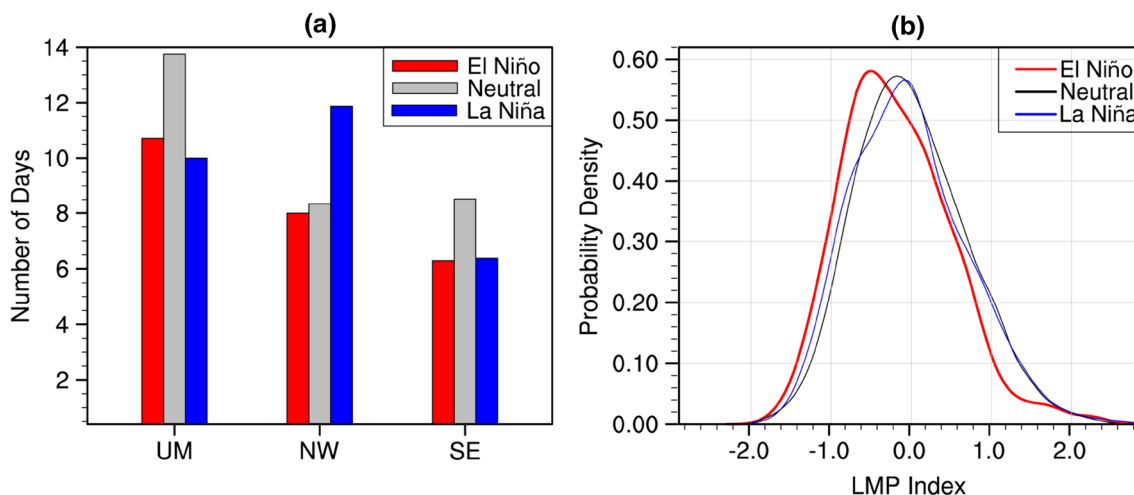


**Fig. 7** **a** The relative frequency of the three ECW groups during different phases of ENSO. **b** PDFs of LMP index for the NW-ECW group during different phases of ENSO. Thin curves signify they are not significantly different from each other at 95% confidence

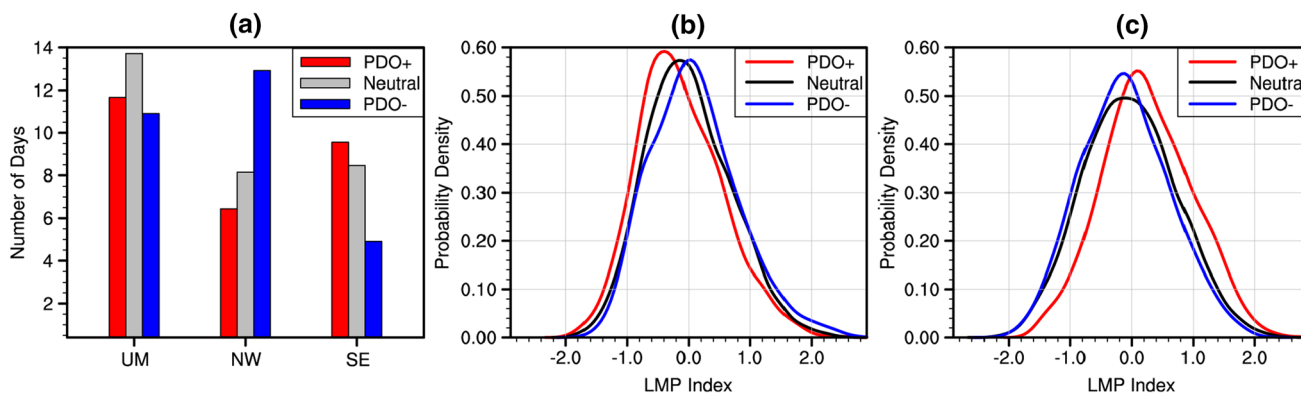


**Fig. 8** a The relative frequency of the three ECW groups during different phases of PDO. PDFs of LMP indexes for **b** the NW- and **c** the SE-ECW groups during different phases of PDO

are most strongly impacted by the PDO phase, occurring most frequently during the negative phase of PDO at 95% confidence. In a consistent manner, the PDF of NW LMP index (Fig. 8b) is right-shifted (more positive) during the negative PDO phase. Thus, during the negative PDO phase the frequency of NW ECWs is modulated via the NW LMP. Similarly, SE ECWs are significantly favored during the positive PDO phase. Correspondingly, the PDF of SE LMP index is significantly right-shifted (more positive) during the positive PDO phase (Fig. 8c). We suggest that the PDO thus modulates SE-ECW frequency via changes in the population of SE LMP. This confirms the results of Westby et al. (2013), who suggest that the PDO might influence US ECWs.

**4.3 Association with Arctic SIE**

Figure 9 displays the occurrence of ECWs and PDFs for NW and SE LMP indexes stratified according to Arctic SIE phase for the boreal cool season. It is clear from

Fig. 9a that years with relatively high (low) SIE tend to weakly favor the occurrence of the UM and NW (SE) ECWs. Considering the PDFs of UM and NW LMP indexes, differences among PDFs are only found for the NW LMP index (Fig. 9b). Though NW LMP index PDF is not significantly different during high SIE years versus neutral years, the PDF is left-shifted (more negative) during less sea ice. The results suggest that less sea ice likely affects NW-ECW frequency. In contrast, the SE LMP index PDF (Fig. 9c) is clearly right-shifted (more positive). This result suggests that less sea ice preferentially favors the occurrence of SE ECWs. This agrees, to some extent, with the results of Francis and Vavrus (2012), who showed that sea-ice loss contributes to weakened zonal winds and intensified meridional circulation features, thereby inducing extreme weather events.

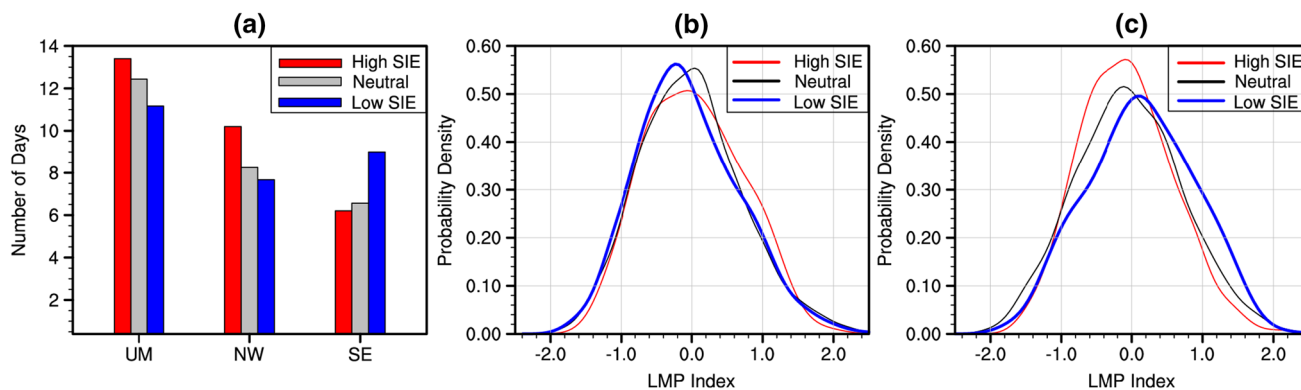


**Fig. 9** a The relative frequency of the three ECW groups during different phases of Arctic SIE. PDFs of LMP indexes for **b** the NW- and **c** the SE-ECW groups during different phases of Arctic SIE. Thin

curves signify they are not significantly different from one another at 95% confidence

#### 4.4 Association with Eurasian SCE

Figure 10 displays the occurrence of ECWs and PDFs of UM and SE LMP indexes for the boreal cool season stratified according to Eurasian SCE phase. In contrast to the results for SIE, the UM and SE ECWs are marginally more frequent during high SCE years (Fig. 10a). In a consistent fashion, both the UM and SE LMP PDFs are substantially right-shifted during high SCE years (Fig. 10b, c). Thus, high Eurasian SCE during the cool season favors the occurrence of UM and SE ECWs. The results are in good agreement with the findings of Cohen et al. (2007). However, Cohen et al. (2007) tied the negative NAM phase, which favors enhanced ECW occurrence over southeastern US (Loikith and Broccoli 2014), to October SCE, while in the present study we consider the cool-season SCE.

### 5 Summary and discussion

We have systematically investigated different types of extreme cold wave events (ECWs) in the conterminous US, along with their associated intraseasonal large-scale meteorology patterns (LMPs), occurring during the boreal cool season for the period 1950–2005. We have also studied the representation of ECWs and LMPs in parallel historical simulations of CCSM4. We further examine linkages among ECWs, LMP and anomalous remote forcing. Using cluster analysis, ECWs are classified into three distinct groups, characterized by negative surface air temperature (SAT) anomaly patterns centered over the upper midwest (UM), northwestern (NW) US, and southeastern (SE) US, respectively (denoted UM ECWs, NW ECWs and SE ECWs). All three ECW types are synoptically characterized by anomalous surface high pressure concentrated near and to west of the SAT

anomaly pattern center. In the mid-troposphere, the UM LMP features a dipole structure with a positive height anomaly over Alaska and a negative height anomaly over central and eastern North America. The NW LMP is a remotely-forced quasi-zonal wave train of height anomalies extending from near Alaska through North America into the North Atlantic. The SE LMP is qualitatively anti-symmetric with respect to the NW LMP.

The basic patterns of SAT anomalies, surface synoptic features, and LMPs are generally well represented in the CCSM4 simulation, with some regional deficiencies in amplitude and the relative ECW frequency. For the UM- and NW-ECW groups, the model-simulated SAT and SLP anomaly patterns are higher in amplitude than for observed events. In contrast, the circulation amplitude for the SE-ECW group is under-represented in CCSM4. The CCSM4 reproduces more NW- and SE-ECW days and fewer UM-ECW days than found in observations. The CCSM4 also reproduces the observed enhancement in LMP frequency during ECWs. Therefore, the NW and SE ECWs are overpopulated by CCSM4, while the UM-ECW group is underpopulated.

Remote forcing exerts a varied impact upon the ECW groups via planetary waves. La Niña favors the occurrence of NW ECWs. Similarly the negative (positive) phase of Pacific Decadal Oscillation tends to induce more frequent NW (SE) ECWs. Both low Arctic sea ice extent (SIE) and high Eurasian snow cover extent (SCE) are associated with more frequent SE ECWs. Also, high Eurasian SCE acts to increase the occurrence of UM-ECWs. The high Eurasian SCE serves to regionally cool the atmosphere, inducing negative height anomalies, while the low Arctic SIE warms the atmosphere resulting in high latitude positive height anomalies. As a result, westerly winds at high latitudes are weakened leading to more frequent cold air outbreaks in the southeast US. Our

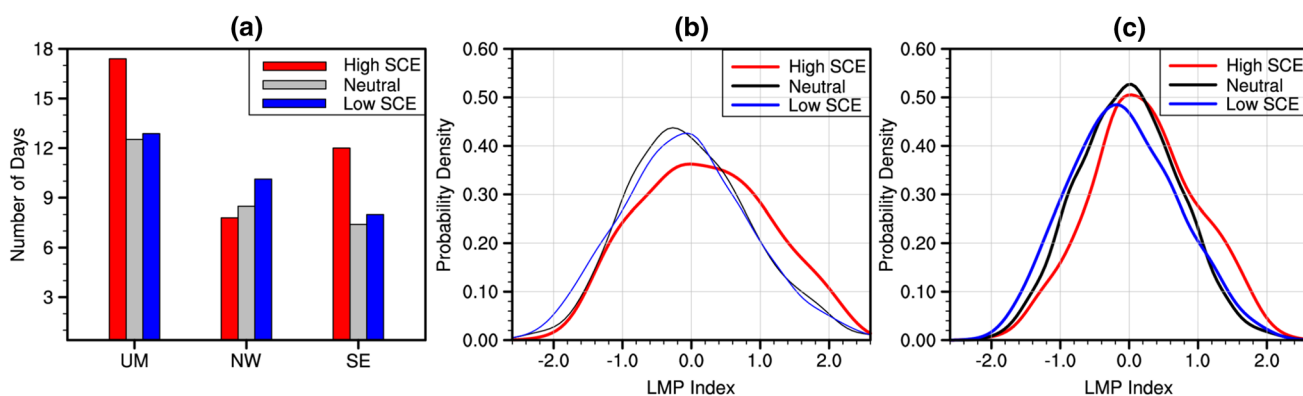


**Fig. 10** a The relative frequency of the three ECW groups during different phases of Eurasian SCE. PDFs of LMP indexes for b the UM- and c the SE-ECW groups during different phases of Eurasian

SCE. Thin curves signify they are not significantly different from one another at 95% confidence

results are generally consistent with prior studies (Francis and Vavrus 2012; Westby et al. 2013; Loikith and Broccoli 2014; Westby and Black 2015).

This study has mainly focused on characterizing the circulation features of the ECW groups, and their associated linkage to anomalous remote forcing, with the related dynamics responsible for ECW time evolution and linkages to circulations of larger scales as yet unexplored. Since LMP structures vary among the three ECW groups with noted differences in Rossby wave activity flux signatures, the formation and maintenance mechanisms likely correspondingly vary. To address these outstanding scientific issues, our future research will more fully explore the mechanistic life cycles of the ECW LMPs via the application of piecewise tendency diagnosis (Evans and Black 2003). These diagnostic analyses will focus on isolating the physical mechanisms underlying the linkages among ECWs, LMP and remote forcing identified in the current study.

**Acknowledgements** We thank the anonymous reviewers for their insightful suggestions and comments. This work was supported by the U.S. Department of Energy, Office of Biological and Environmental Research, Awards DE-SC0012554. Yi Deng is also partly supported by the National Science Foundation Climate and Large-Scale Dynamics (CLD) program through Grants AGS-1147601, AGS-1354402, and AGS-1445956. The authors thank writers of the NCAR Command Language (UCAR/NCAR/CISL/TDD 2016) and Matlab, which were employed to perform cluster analysis and plot the figures.

## References

- Bosart LF, Papin PP, Bentley AM, Moore BJ, Winters AC (2015) Large-scale antecedent conditions associated with 2014–2015 winter onset over North America and mid-winter storminess along the North Atlantic coast. In: American Geophysical Union 2015 Fall Meeting. 14–18 December 2015. <https://agu.confex.com/agu/fm15/meetingapp.cgi/Paper/48384>. Accessed 17 Dec 2015
- Bueh C, Shi N, Xie Z (2011) Large-scale circulation anomalies associated with persistent low temperature over Southern China in January 2008. *Atmos Sci Lett* 12:273–280. doi:10.1002/asl.333
- Carrera ML, Higgins RW, Kousky VE (2004) Downstream weather impacts associated with atmospheric blocking over the Northeast Pacific. *J Clim* 17:4823–4839. doi:10.1175/JCLI-3237.1
- Cohen J, Barlow M, Kushner PJ, Saito K (2007) Stratosphere-troposphere coupling and links with Eurasian land surface variability. *J Clim* 20:5335–5343. doi:10.1175/2007JCLI1725.1
- Cohen J, Screen JA, Furtado JC, Barlow M, Whittleston D, Coumou D, Francis J, Dethloff K, Entekhabi D, Overland J, Justin J (2014) Recent Arctic amplification and extreme mid-latitude weather. *Nat Geosci* 7:627–637. doi:10.1038/ngeo2234
- Evans KJ, Black RX (2003) Piecewise tendency diagnosis of weather regime transitions. *J Atmos Sci* 60:1941–1959
- Fetterer F, Knowles K, Meier W, Savoie M (2002) Updated daily. Sea Ice Index, Version 1. [indicate subset used]. Boulder, Colorado USA. NSIDC: National Snow and Ice Data Center. doi:10.7265/N5QJ7F7W
- Francis JA, Vavrus SJ (2012) Evidence linking Arctic amplification to extreme weather in mid-latitudes. *Geophys Res Lett*. doi:10.1029/2012GL051000
- Gent PR, Danabasoglu G, Donner LJ, Holland MM, Hunke EC, Jayne SR, Lawrence DM, Neale RB, Rasch PJ, Vertenstein M, Worley PH, Yang ZL, Zhang M (2011) The community climate system model version 4. *J Clim* 24:4973–4991. doi:10.1175/2011JCLI4083.1
- Grotjahn R, Faure G (2008) Composite predictor maps of extraordinary weather events in the Sacramento, Weather Forecast, California, region 23:313–335.
- Grotjahn R, Barlow M, Black R, Cavazos T, Gutowski W, Gyakum J, Katz R, Kumar A, Leung LY, Schumacher R, Wehner M (2014) Workshop on analyses, dynamics, and modeling of large-scale meteorological patterns associated with extreme temperature and precipitation events. [https://usclivar.org/sites/default/files/documents/2014/2013\\_Extremes\\_Workshop\\_Report.pdf](https://usclivar.org/sites/default/files/documents/2014/2013_Extremes_Workshop_Report.pdf). Accessed 1 June 2014
- Grotjahn R, Black R, Leung R, Wehner MF, Barlow M, Bosilovich M, Gershunov A, Gutowski Jr WJ, Gyakum JR, Katz RW, Lee YY, Lim YK, Prabhat (2015) North American extreme temperature events and related large scale meteorological patterns: a review of statistical methods, dynamics, modeling, and trends. *Clim Dyn* 46:1151–1184. doi:10.1007/s00382-015-2638-6
- Hartmann DL (2015) Pacific sea surface temperature and the winter of 2014. *Geophys Res Lett* 42:1894–1902
- Huang B, Banzon VF, Freeman E, Lawrimore J, Liu W, Peterson TC, Smith TM, Thorne PW, Woodruff SD, Zhang HM (2015) Extended reconstructed sea surface temperature version 4 (ERSST.v4): Part I. upgrades and intercomparisons. *J Clim* 28:911–930. doi:10.1175/JCLI-D-14-00006.1
- IPCC (2012) Managing the risks of extreme events and disasters to advance climate change adaptation. In: Field CB, Barros V, Stocker TF, Qin D, Dokken DJ, Ebi KL, Mastrandrea MD, Mach KJ, Plattner GK, Allen SK, Tignor M, Midgley PM (eds), A Special Report of Working Groups I and II of the Intergovernmental Panel on Climate Change. Cambridge University Press, Cambridge
- Kalnay E, Kanamitsu M, Kistler R, Collins W, Deaven D, Gandin L, Iredell M, Saha S, White G, Woollen J, Zhu Y, Chelliah M, Ebisuzaki W, Higgins W, Janowiak J, Mo KC, Ropelewski C, Wang J, Leetmaa A, Reynolds R, Jenne R, Joseph D (1996) The NCEP/NCAR 40-year reanalysis project. *Bull Am Meteorol Soc* 77:437–471
- Kenyon J, Hegerl GC (2008) Influence of modes of climate variability on global temperature extremes. *J Clim* 21:3872–3889. doi:10.1175/2008JCLI2125.1
- Konrad CE II (1996) Relationships between the intensity of cold-air outbreaks and the evolution of synoptic and planetary-scale features over North America. *Mon Weather Rev* 124:1067–1083
- Kug JS, Jeong JH, Jang YS, Kim BM, Folland CK, Min SK, Son SW (2015) Two distinct influences of Arctic warming on cold winters over North America and East Asia. *Nat Geosci* 8:759–762. doi:10.1038/ngeo2517
- Liu J, Curry JA, Wang H, Song M, Horton RM (2012) Impact of declining Arctic sea ice on winter snowfall. *Proc Natl Acad Sci* 109:4074–4079
- Loikith PC, Broccoli AJ (2012) Characteristics of observed atmospheric circulation patterns associated with temperature extremes over North America. *J Clim* 25:7266–7281. doi:10.1175/JCLI-D-11-00709.1
- Loikith PC, Broccoli AJ (2014) The influence of recurrent modes of climate variability on the occurrence of winter and summer extreme temperatures over North America. *J Clim* 27:1600–1618

- Park TW, Ho CH, Deng Y (2013) A synoptic and dynamical characterization of wave-train and blocking cold surge over East Asia. *Clim Dyn* 43:753–770
- Robinson DA, Dewey KF, Heim RRJ (1993) Global snow cover monitoring: an update. *Bull Am Meteorol Soc* 74:1689–1696. doi:10.1175/1520-0477(1993)074<1689:GSCMAU>2.0.CO;2
- Sillmann J, Kharin VV, Zhang X, Zwiers FW, Bronaugh D (2013) Climate extremes indices in the CMIP5 multimodel ensemble: Part I. model evaluation in the present climate. *J Geophys Res* 118:1716–1733
- Stan C, Straus DM (2007) Is blocking a circulation regime? *Mon Weather Rev* 135:2406–2413
- Takaya K, Nakamura H (2001) A formulation of a phase-Independent wave-activity flux for stationary and migratory quasigeostrophic eddies on a zonally varying basic flow. *J Atmos Sci* 58:608–627
- Trenary L, Delsole T, Tippett MK et al (2015) Was the cold eastern US winter of 2014 due to increase vairabilty? [in “Explaining Extremes of 2014 from a Climate Perspective”]. *Bull Am Meteorol Soc* 96 (12):S15–S19
- UCAR/NCAR/CISL/TDD (2016) The NCAR Command Language (Version 6.3.0) [Software]. UCAR/NCAR/CISL/TDD, Boulder. doi:10.5065/D6WD3XH5
- Ward JH (1963) Hierarchical grouping to optimize an objective function. *J Am Stat Assoc* 58:236–244. doi:10.1080/01621459.1963.10500845
- Westby RM, Black RX (2015) Development of anomalous temperature regimes over the southeastern United States: synoptic behavior and role of low-frequency modes. *Weather Forecast* 30:553–570. doi:10.1175/WAF-D-14-00093.1
- Westby RM, Lee YY, Black RX (2013) Anomalous temperature regimes during the cool season: long-term trends, low-frequency mode modulation, and representation in CMIP5 simulations. *J Clim* 26:9061–9076. doi:10.1175/JCLI-D-13-00003.1
- Whan K, Zwiers F, Sillmann J (2016) The Influence of Atmospheric Blocking on Extreme Winter Minimum Temperatures in North America. *J Clim* 29:4361–4381. doi:10.1175/JCLI-D-15-0493.1
- Wilks DS (2006) *Statistical methods in the atmospheric sciences*, 2nd. Academic Press, Waltham
- WMO (2012) Cold spell in Europe and Asia in late winter 2011/2012. WMO Regional Climate Centres, 20 pp. [https://ane4bf-datap1.s3-eu-west-1.amazonaws.com/wmocms/s3fpublic/news/related\\_docs/dwd\\_2012\\_report.pdf](https://ane4bf-datap1.s3-eu-west-1.amazonaws.com/wmocms/s3fpublic/news/related_docs/dwd_2012_report.pdf). Accessed 12 Mar 2012
- Wolter K, Hoerling M, Eischeid JK, Olderborgh GJV, Quan XW, Walsh JE, Chase TN, Dole RM (2015) How unusual was the cold winter of 2013/14 in the upper midwest? [in “Explaining Extremes of 2014 from a Climate Perspective”]. *Bull Am Meteorol Soc* 96 (12):S10–S14
- Zhao S, Deng Y, Black RX (2016) Warm season dry spells in the central and eastern United States: diverging skill in climate model representation. *J Clim* 29:5617–5624. doi:10.1175/JCLI-D-16-0321.1